Research Article | Vol. 24, No. 15 | 25 Jul 2016 | OPTICS EXPRESS 16973

Optics EXPRESS

Mid-infrared dual-gas sensor for simultaneous detection of methane and ethane using a single continuous-wave interband cascade laser

Weilin Ye,[1,2,6] Chunguang Li,[1,3,6] Chuantao Zheng,[1,3,*] Nancy P. Sanchez,[4] Aleksander K. Gluszek,[1] Arkadiusz J. Hudzikowski,[1] Lei Dong,[1,5] Robert J. Griffin,[4] and Frank K. Tittel[1]

[1]*Department of Electrical and Computer Engineering, Rice University, 6100 Main Street, Houston, Texas 77005, USA*
[2]*College of Engineering, Shantou University, 243 Daxue Road, Shantou 515063, China*
[3]*State Key Laboratory on Integrated Optoelectronics, College of Electronic Science and Engineering, Jilin University, 2699 Qianjin Street, Changchun 130012, China*
[4]*Department of Civil and Environmental Engineering, Rice University, 6100 Main Street, Houston, Texas 77005, USA*
[5]*State Key Laboratory of Quantum Optics and Quantum Optics Devices, Institute of Laser Spectroscopy, Shanxi University, Taiyuan 030006, China*
[6]*W. Ye and C. Li contributed equally to this work*
[*]*zhengchuantao@jlu.edu.cn*

Abstract: A continuous-wave (CW) interband cascade laser (ICL) based mid-infrared sensor system was demonstrated for simultaneous detection of atmospheric methane (CH_4) and ethane (C_2H_6). A 3.337 μm CW ICL with an emitting wavenumber range of 2996.0–3001.5 cm^{-1} was used to simultaneously target two absorption lines, C_2H_6 at 2996.88 cm^{-1} and CH_4 at 2999.06 cm^{-1}, respectively. The sensor performance was first evaluated for single-gas detection by only targeting the absorption line of one gas species. Allan deviations of 11.2 parts per billion in volume (ppbv) for CH_4 and 1.86 ppbv for C_2H_6 with an averaging time of 3.4 s were achieved for the detection of these two gases. Dual-gas detection was realized by using a long-term scan signal to target both CH_4 and C_2H_6 lines. The Allan deviations increased slightly to 17.4 ppbv for CH_4 and 2.4 ppbv for C_2H_6 with an averaging time of 4.6 s due to laser temperature and power drift caused by long-term wavelength scanning. Measurements for both indoor and outdoor concentration changes of CH_4 and C_2H_6 were conducted. The reported single ICL based dual-gas sensor system has the advantages of reduced size and cost compared to two separate sensor systems.

OCIS codes: (280.3420) Laser sensors; (300.6340) Spectroscopy, infrared; (140.5965) Semiconductor lasers, quantum cascade.

References and Links

1. I. Bamberger, J. Stieger, N. Buchmann, and W. Eugster, "Spatial variability of methane: Attributing atmospheric concentrations to emissions," Environ. Pollut. **190**, 65–74 (2014).
2. F. A. Smith, S. Elliott, D. R. Blake, and F. S. Rowland, "Spatiotemporal variation of methane and other trace hydrocarbon concentrations in the Valley of Mexico," Environ. Sci. Policy **5**(6), 449–461 (2002).
3. I. J. Simpson, F. S. Rowland, S. Meinardi, and D. R. Blake, "Influence of biomass burning during recent fluctuations in the slow growth of global tropospheric methane," Geophys. Res. Lett. **33**(22), L22808 (2006).
4. Y. Xiao, J. A. Logan, D. J. Jacob, R. C. Hudman, R. Yantosca, and D. R. Blake, "Global budget of ethane and regional constraints on U.S. sources," J. Geophys. Res. **113**(D21), D21306 (2008).
5. G. Etiope and P. Ciccioli, "Earth's degassing: a missing ethane and propane source," Science **323**(5913), 478 (2009).
6. P. Paredi, S. A. Kharitonov, and P. J. Barnes, "Elevation of exhaled ethane concentration in asthma," Am. J. Respir. Crit. Care Med. **162**(4), 1450–1454 (2000).

#267743 http://dx.doi.org/10.1364/OE.24.016973
Journal © 2016 Received 6 Jun 2016; revised 13 Jul 2016; accepted 14 Jul 2016; published 18 Jul 2016
Corrected: 19 July 2016

Optics EXPRESS

7. B. K. Puri, B. M. Ross, and I. H. Treasaden, "Increased levels of ethane, a non-invasive, quantitative, direct marker of n-3 lipid peroxidation, in the breath of patients with schizophrenia," Prog. Neuropsychopharmacol. Biol. Psychiatry **32**(3), 858–862 (2008).
8. K. D. Skeldon, L. C. McMillan, C. A. Wyse, S. D. Monk, G. Gibson, C. Patterson, T. France, C. Longbottom, and M. J. Padgett, "Application of laser spectroscopy for measurement of exhaled ethane in patients with lung cancer," Respir. Med. **100**(2), 300–306 (2006).
9. D. G. Lancaster, R. Weidner, D. Richter, F. K. Tittel, and J. Limpert, "Compact CH_4 sensor based on difference frequency mixing of diode lasers in quasi-phasematched $LiNbO_3$," Opt. Commun. **175**(4-6), 461–468 (2000).
10. D. G. Lancaster and J. M. Dawes, "Methane detection with a narrow-band source at 3.4 μm based on a Nd:YAG pump laser and a combination of stimulated Raman scattering and difference frequency mixing," Appl. Opt. **35**(21), 4041–4045 (1996).
11. C. Fischer and M. W. Sigrist, "Trace-gas sensing in the 3.3-μm region using a diode-based difference-frequency laser photoacoustic system," Appl. Phys. B-Lasers **75**(2–3), 305–310 (2002).
12. D. Richter, D. G. Lancaster, R. F. Curl, W. Neu, and F. K. Tittel, "Compact mid-infrared trace gas sensor based on difference-frequency generation of two diode lasers in periodically poled $LiNbO_3$," Appl. Phys. B-Lasers **67**(3), 347–350 (1998).
13. K. P. Petrov, S. Waltman, E. J. Dlugokencky, M. Arbore, M. M. Fejer, F. K. Tittel, and L. W. Hollberg, "Precise measurement of methane in 3.4-μm difference-frequency generation in PPLN," Appl. Phys. B-Lasers **4**(5), 567–572 (1997).
14. J. A. Silver, "Frequency-modulation spectroscopy for trace species detection: theory and comparison among experimental methods," Appl. Opt. **31**(6), 707–717 (1992).
15. P. Werle, "A review of recent advances in semiconductor laser based gas monitors," Spectrochim. Acta A **54**(2), 197–236 (1998).
16. S. Schilt, L. Thévenaz, and P. Robert, "Wavelength modulation spectroscopy: combined frequency and intensity laser modulation," Appl. Opt. **42**(33), 6728–6738 (2003).
17. J. Li, U. Parchatka, and H. Fischer, "A formaldehyde trace gas sensor based on a thermoelectrically cooled CW-DFB quantum cascade laser," Anal. Methods **6**(15), 5483–5488 (2014).
18. J. H. Miller, Y. A. Bakhirkin, T. Ajtai, F. K. Tittel, C. J. Hill, and R. Q. Yang, ""Detection of formaldehyde using off-axis integrated cavity output spectroscopy with an interband cascade laser," Appl. Phys. B-Lasers **85**(2–3), 391–396 (2006).
19. T. I. Yacovitch, S. C. Herndon, J. R. Roscioli, C. Floerchinger, R. M. McGovern, M. Agnese, G. Pétron, J. Kofler, C. Sweeney, A. Karion, S. A. Conley, E. A. Kort, L. Nähle, M. Fischer, L. Hildebrandt, J. Koeth, J. B. McManus, D. D. Nelson, M. S. Zahniser, and C. E. Kolb, "Demonstration of an Ethane Spectrometer for Methane Source Identification," Environ. Sci. Technol. **48**(14), 8028–8034 (2014).
20. C. Li, L. Dong, C. Zheng, and F. K. Tittel, "Compact TDLAS based optical sensor for ppb-level ethane detectionby use of a 3.34 m room-temperature CW interband cascade laser," Sensor. Actuat. Biol. Chem. **232**, 188–194 (2016).
21. L. Dong, C. Li, N. P. Sanchez, A. K. Gluszek, R. Griffin, and F. K. Tittel, "Compact CH_4 sensor system based on a continuous-wave, low power consumption, room temperature interband cascade laser," Appl. Phys. Lett. **108**(1), 011106 (2016).
22. K. Liu, T. Liu, J. Jiang, G. D. Peng, H. Zhang, D. Jia, Y. Wang, W. Jing, and Y. Zhang, "Investigation of wavelength modulation and wavelength sweep techniques in intracavity fiber laser for gas detection," J. Lightwave Technol. **29**(1), 15–21 (2011).
23. R. Arndt, "Analytical line shapes for Lorenzian signals broadened by modulation," J. Appl. Phys. **36**(8), 2522–2524 (1965).
24. J. Reid and D. Labrie, ""Second harmonic detection with tunable diode lasers-comparison of experiment and theory," Appl. Phys. B-Lasers **26**(3), 203–210 (1981).

1. Introduction

Methane (CH_4) is a key contributor to the greenhouse effect and a safety hazard in several industries, including natural gas production, distribution and storage, transportation, coal mining, and the handling of liquefied CH_4. Hence, it is important to monitor CH_4 in both urban and rural areas [1–3]. Ethane (C_2H_6), which is the second-largest component of natural gas after CH_4, is predominantly used in the chemical industry, for example in the production of ethylene (C_2H_4) by steam cracking or as a feedstock in the manufacture of other commodity chemicals. In the Earth's atmosphere, the CH_4 concentration level is ~1.8 parts per million by volume (ppmv), and C_2H_6 occurs as a trace gas at concentration levels of several parts per billion by volume (ppbv). Furthermore, ultra-sensitive C_2H_6 detection has found applications in human breath analysis as a non-invasive method to monitor and identify different diseases, such as lung cancer and asthma. Therefore, the detection of CH_4 and C_2H_6

Optics EXPRESS

is important in environmental monitoring and atmospheric chemistry [4,5] as well as industrial process control and breath analysis [6–8].

In comparison with mass spectrometry or gas chromatography, optical methods based on infrared laser spectroscopy [9–13] are advantageous for CH_4 and C_2H_6 sensing in terms of size, cost and requiring no pretreatment and accumulation of the concentration of the targeted gas samples. In addition, optical methods provide high-precision remote sensing capabilities and fast response. Tunable infrared diode laser absorption spectroscopy (TDLAS) [14–16] enables non-contact measurements and has proven to be an excellent tool for trace gas detection in various applications. TDLAS requires a tunable laser exhibiting single frequency emission and a narrow linewidth at the targeted absorption line of a gas molecule in order to achieve high detection sensitivity and selectivity in the near and mid-infrared spectral range. Quantum cascade lasers (QCLs) [17] in the 4–12 μm spectral range and interband cascade lasers (ICLs) in the 2.5–4 μm spectral range with low power-consumption [18] are lasers of optimum choice in TDLAS, because they provide advantages of continuous-wave (CW) output power levels (up to ~hundreds of mW for QCLs and ~tens of mW for ICLs).

Simultaneous detection of C_2H_6 and CH_4 is an effective method to discriminate CH_4 origin between thermogenic (e.g. natural gas production) and biogenic sources (e.g. landfills, wetlands). Thermogenic CH_4 usually contains a varying concentration of C_2H_6 according to its origin and degree of processing (e.g. dry and wet natural gas), while CH_4 derived from microbial action is not accompanied by C_2H_6 formation [19]. In previous studies, two separate ICL based sensors operating at 3291 nm and 3337 nm were developed [20,21] and demonstrated for monitoring CH_4 leakage at natural gas vehicle fueling stations. TDLAS for CH_4 detection and wavelength modulation spectroscopy (WMS) for C_2H_6 detection were employed in several field campaigns. However, the two sensor systems required two data acquisition (DAQ) cards, two vacuum pumps, two pressure controllers, a lock-in amplifier, QCL and ICL current drivers and temperature controllers. This equipment required a large-sized vehicle for mobile deployment of these sensor units and represented high power-consumption by the two sensor systems. Limited power of large-sized batteries impacted the continuity of long-term field monitoring campaigns. Therefore, a compact dual-gas CH_4/C_2H_6 sensor intended to overcome these limitations was developed. A single ICL emitting at 3.337 μm was selected based on a detailed high resolution transmission (HITRAN) spectral analysis to target CH_4 and C_2H_6 absorption lines for dual-gas detection. Furthermore, a LabVIEW based data-processing system, which consists of a scan and modulation signal generator, a signal acquisition module and a lock-in amplifier was developed. Such a system can perform the normal operation of driving an ICL as well as extracting the CH_4 and C_2H_6 harmonic signals from the absorption spectra employing a laptop and a DAQ card.

2. Dual-gas sensor configuration

2.1 Sensor architecture

The dual-gas CH_4/C_2H_6 sensor architecture is depicted in Fig. 1, which includes an optical and an electrical sub-system. In the optical part, a Nanoplus CW, thermoelectrically cooled (TEC) ICL was used as the excitation source, which has an operation temperature range of 5–15 °C. The current and temperature tuning coefficient for this ICL were measured to be −0.141528 cm^{-1}/mA and −0.30138 cm^{-1}/°C, respectively. A dichroic mirror (DM, ISP Optics, model BSP-DI-25-3) was used to combine a visible alignment diode laser beam with the mid-infrared ICL beam. The combined beams were coupled to the 54.6 m multi-pass gas cell (MPGC, physical size: 17 × 6.5 × 5.5 cm^3, Sentinel Photonics/Aries Technologies) using a CaF_2 lens and two adjustable plane mirrors (M1 and M2). The CaF_2 lens has a focal length of 20 cm and no anti-reflection (AR) coatings. The lens was placed after the DM to focus the two laser beams into the MPGC to meet the pattern-size requirement of the MPGC. The beam entered the gas cell and exited after 453 reflections. The output beam was focused onto a TEC

Optics EXPRESS

mercury-cadmium-telluride (MCT) photodetector (VIGO System, model PVI-4TE-3.4) using a parabolic mirror (PM). All the optical elements were mounted on an aluminum plate, in order to reduce the sensor size and weight without degrading sensor-system performance for field deployment. The alignment of the beam was performed at laboratory temperature (~25 °C) to achieve an exact absorption path length of 54.6 m. The cell temperature was not stabilized during the experiment, but was limited within a range of 20 – 30 °C. Preliminary tests indicate that temperature levels above 35 °C will vary the absorption path length and the MPGC beam pattern, impacting the proper operation of the sensor unit.

The electrical part of the sensor system consists of a laptop (Dell, model # PP04X), a DAQ card (National Instrument, model USB-6356), an integrated laser current driver and a temperature controller (Wavelength Electronics, model 0520). The laser current driver has a size of 8 × 5 × 3 cm^3 and a 5 V supply voltage. The ratio between input voltage and output current was adjusted to 20 mA/V by means of an external circuit to improve the current accuracy. A WMS technique was used for CH_4/C_2H_6 detection, which requires a scan signal as well as a modulation signal to drive the ICL laser. These two signals were generated by a LabVIEW controlled DAQ card. Furthermore, the MCT detector signal was sent to the DAQ for data acquisition triggered by the signal generation module. A LabVIEW based lock-in amplifier was developed and used to extract the harmonic signals, through the use of two frequency-doubled orthogonal signals as two reference signals. In addition, a compact, oil-free vacuum pump (KNF Neuberger Inc., model N 813.5 ANE/AF) and a pressure controller (MKS Instruments, Inc., Type 649) were used to pump the target gases into the MPGC and to control the gas pressure inside the MPGC, respectively.

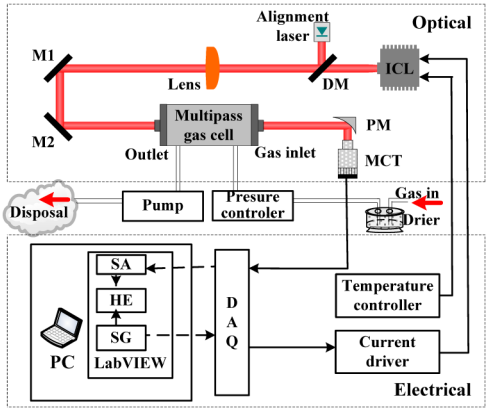

Fig. 1. Schematic of the dual-gas CH_4/C_2H_6 sensor based on a single CW, TEC ICL. ICL: interband cascade laser; DM: dichroic mirror; M: plane mirror; PM: parabolic mirror; MCT: mercury-cadmium-telluride. SA: signal acquisition; HE: harmonic extraction; SG: signal generation.

2.2 C_2H_6/CH_4 line selection

Both CH_4 and C_2H_6 have strong absorption bands near 3.34 μm. At this wavelength, the potential spectral interference originates mainly from water (H_2O), which will affect the CH_4 and C_2H_6 detection. HITRAN absorption spectra of 10 ppbv C_2H_6, 2 ppmv CH_4, and 2% H_2O calculated at 100 Torr gas pressure and a 5460 cm effective optical path length are depicted in Fig. 2(a). An interference-free C_2H_6 absorption line centered at 3336.8 nm (2996.88 cm^{-1}) was selected as the optimum target line. There are two strong absorption lines located at 2998.99 cm^{-1} and 2999.06 cm^{-1}, which can be distinguished at reduced pressure (e.g. 100 Torr) without line broadening. However, two H_2O lines (2998.97 cm^{-1} and 2999.16 cm^{-1}) were found to be located close to the two CH_4 lines. In view of the fact that the 2998.97 cm^{-1} H_2O line almost overlaps with the 2998.99 cm^{-1} CH_4 line, we selected the 2999.06 cm^{-1} CH_4

Optics EXPRESS

line for optimum detection. Also, a low H_2O concentration, e.g. < 2%, was required to minimize its effect on CH_4 detection, which was realized by using a H_2O trap based on calcium sulfate (W.A. Hammond Drierite, CAS# 7778-18-9). Generally, the drier can reduce the H_2O concentration to < 0.1%. The H_2O concentration varies with ambient conditions. However, because the water absorption line at 2999.06 cm^{-1} is flat at concentration levels of < 0.1%, the absorption caused by water can be treated as background information. Hence a change of the H_2O concentration level within 0 – 0.1% will cause no effect on CH_4 detection. The drier needs to be replaced periodically for long-term measurements to ensure a relative H_2O concentration of < 0.1%. Figure 2(b) shows a plot of the ICL emission wavenumber as a function of the ICL drive current at an operating temperature of 10 °C. To target both the 2999.06 cm^{-1} CH_4 and the 2996.88 cm^{-1} C_2H_6 absorption lines, the drive current should be 32 and 47 mA, respectively.

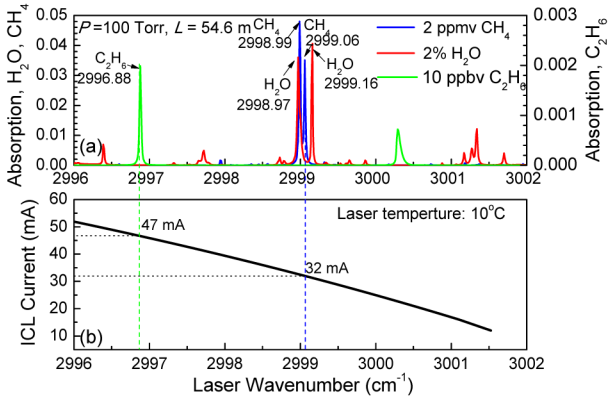

Fig. 2. (a) HITRAN based absorption spectra of C_2H_6 (10 ppbv), CH_4 (2 ppmv), and H_2O(2%) in a narrow spectral range from 2996 cm^{-1} to 3002 cm^{-1} at a pressure of 100 Torr and an absorption length of 54.6 m. C_2H_6, CH_4, and H_2O lines are shown in green, blue and red, respectively. (b) Plot of the ICL emission wavenumber as a function of the ICL drive current at 10 °C.

2.3 LabVIEW-based data-processing system

A LabVIEW based laptop platform was developed, whose function diagram is shown in Fig. 3. There are three main functions of this platform: signal generation (SG), signal acquisition (SA) and harmonic extraction (HE). For the SG sub-system, both a modulation-signal array and a scan-signal array were generated and superimposed on each other. The superimposed signal was supplied to a digital-to-analog converter (DAC) module. The drive signal was applied to the ICL via the DAQ card. For the SA, via the use of an analog-to-digital converter (ADC), the output signal from the MCT detector was sampled at the same sampling rate with the DAC. In this case, the total number of the sampling points within a period was equal to that of the drive signal, which was required for lock-in data-processing. For HE, the sampled signal was multiplied by two frequency-doubled orthogonal signals which were synchronized by the modulation signal. With low-pass filtering (LPF), biased adding operation (Bias), and square operation (Squre), two orthogonal components were obtained. The bias should assure two completely positive orthogonal signals before a square operation, which was set to 1 V in this system. Then, using a second adding operation between the two components and a square root (sqrt) operation, the *R* signal was obtained. For easy data processing, we removed the baseline from the *R* signal via a subtraction operation, and the 2*f* signal biased at zero (see Fig. 5) was extracted to determine the gas concentration.

Optics EXPRESS

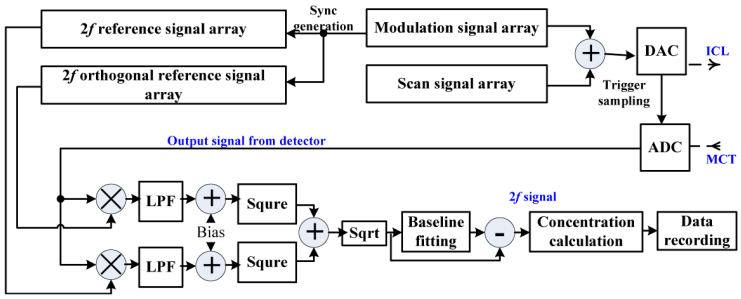

Fig. 3. Function diagram of the LabVIEW-based laptop platform, which performs signal generation, signal acquisition and harmonic extraction.

2.4 Wavelength modulation depth optimization

Theoretically, the optimized modulation depth is 1.1 times of the full width at half-maximum (FWHM) of the absorption line [22–24]. In this work, the wavelength modulation depth was experimentally optimized for a gas pressure of ~100 Torr. The amplitudes of the 2*f* signals were recorded at different modulation amplitudes, as depicted in Fig. 4, where the CH_4 and C_2H_6 concentration levels were 2.1 ppmv and 90 ppbv (achieved by diluting the 1.14 ppmv C_2H_6), respectively. The maximum 2*f* signal of C_2H_6 is achieved at a modulation depth of 0.068 cm^{-1} with a modulation amplitude of ~0.024 V. The maximum 2*f* signal of CH_4 is achieved at a modulation depth of 0.051 cm^{-1} and an amplitude of ~0.020 V. We selected a modulation amplitude of ~0.024 V to enable the design consistency of the sensor system, particularly in terms of the modulation signal generation for CH_4 and C_2H_6.

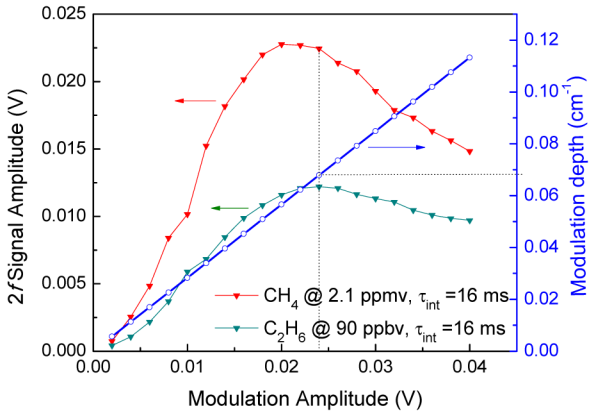

Fig. 4. Measured amplitude of the 2*f* signal and the modulation depth as a function of modulation amplitude for a dry 90 ppbv C_2H_6:N_2 mixture and 2.1 ppmv CH_4:N_2 mixture, where the integration time, τ_{int}, of the LabVIEW based lock-in amplifier was 16 ms, and the modulation frequency was 5 kHz.

3. Single-gas sensing performance

3.1 CH_4 sensing performance

For targeting the CH_4 absorption line at 2999.06 cm^{-1}, the ICL drive current, laser temperature, and the pressure in the MPGC were set to 32 mA, 10 °C and 100 Torr, respectively. The scan signal was a triangular signal with a frequency of 0.3 Hz, a peak-to-peak amplitude of 200 mV and a bias of ~1.6 V. The modulation signal was a sinusoidal signal of 5 kHz with an optimum amplitude of 0.024 V. The integral time of the LabVIEW-based lock-in amplifier was 16 ms. For generating the sinewave signal and improving the

Optics EXPRESS

lock-in resolution, the sampling rate of the DAQ card, including the DAC and ADC module, was set to 300 kHz, resulting in 10^6 data points per triangular period. Sync sampling was realized by using the scan signal of the laser as a triggering signal. Only the first 0.5×10^6 data points were sampled for the first half of a triangular period of ~1.67 s. After that, the 0.5×10^6 data points were sent to the lock-in module. The sampling time plus the data processing time, is ~3.4 s to obtain a 2*f* signal. The recorded 2*f* signals for seven different CH_4 concentration levels of 50, 100, 200, 400, 600, 800 and 1000 ppbv are shown in Fig. 5(a). There were two overlapped harmonic signals and the amplitude of the left one, which has no interference from H_2O, was used for representing CH_4 concentration levels, denoted by $\max_{CH4}(2f)$ in Fig. 5(a).

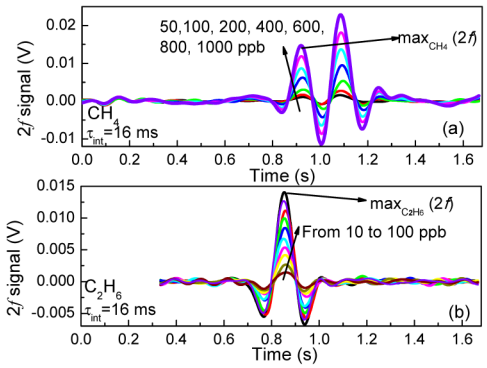

Fig. 5. (a) The recorded 2*f* signal for seven different CH_4 concentration levels of 50, 100, 200, 400, 600, 800 and 1000 ppbv. (b) The recorded 2*f* signal at ten different C_2H_6 concentration levels of 10, 20, 30, 40, 50, 60, 70, 80, 90 and 100 ppbv. The integral time of the LabVIEW-based lock-in amplifier was set at 16 ms, and the modulation frequency was 5 kHz.

With the optimized sensor parameters, CH_4 sensor calibration was carried out by using diluted standard CH_4 gas with eight different concentration levels of 0, 50, 100, 200, 400, 600, 800 and 1000 ppbv, as shown in Fig. 6(a). The amplitude of the 2*f* signal was recorded for ~10 min for each concentration. The measured amplitudes for each concentration was then averaged and plotted as function of CH_4 concentration as shown in Fig. 6(b). The fitting curve indicates a good linear relationship (R-square value: 99.98%) between 2*f* signal and CH_4 concentration, expressed as

$$C = 68.54 \max_{CH_4}(2f) - 0.0184, \text{ in ppmv} \quad (1)$$

The noise level was determined by passing pure N_2 into the gas cell and subsequent monitoring of the detected 2*f* signal amplitude located at the CH_4 peak position. The amplitude can be transformed to CH_4 concentration based on the fitting relation of Eq. (1). A CH_4 concentration measurement of the sample with zero concentration was performed over a time period of ~45 min, as shown in Fig. 6(c). The total variation range of the measured concentration is ~−20–40 ppbv for the 45 min observation time. An Allen-Werle analysis was utilized to evaluate the stability of the CH_4 sensor based on the measured data. As shown in Fig. 6(d), the Allan deviation was plotted on a log-log scale versus the averaging time, τ. The plot indicates a measurement precision of ~11.2 ppbv with a ~3.4 s averaging time. With increasing averaging time, the Allan-Werle plot shows a continuous decrease similar to the decrease of the curve of ~sqrt(1/τ).

3.2 C_2H_6 sensing performance

For targeting the C_2H_6 absorption line of 2996.88 cm^{-1}, the ICL drive current was set to 47 mA. The scan signal was a triangular signal with a frequency of 0.3 Hz, a peak-to-peak amplitude of 200 mV and a bias of ~2.35 V. The same modulation signal and a similar data-

Optics EXPRESS

processing procedure were used as for CH_4 described in Section 3.1. The sampled 2*f* signals for 10 different C_2H_6 concentration levels of 10, 20, 30, 40, 50, 60, 70, 80, 90, 100 ppbv are shown in Fig. 5(b). There were fluctuations in the first part (100 k data points) of the 2*f* signals, so that only the last 400 k data points are shown in Fig. 5(b). The amplitude of the 2*f* signal, denoted by $\max_{C2H6}(2f)$, was used to represent C_2H_6 concentration.

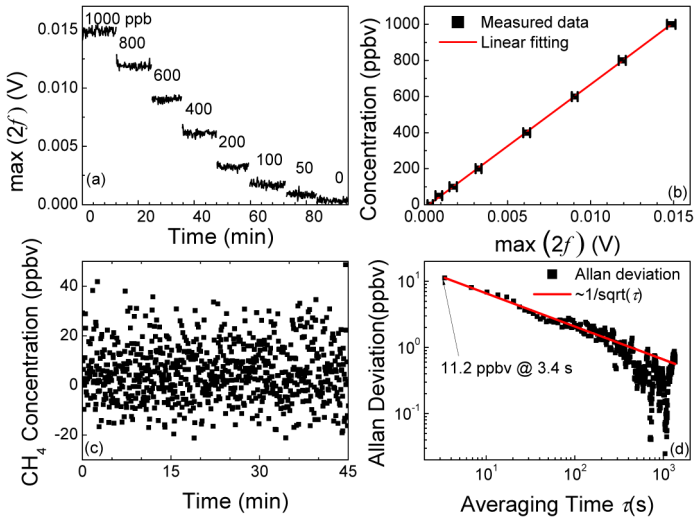

Fig. 6. (a) Measured 2*f* amplitude, max(2*f*), versus calibration time *t* for eight CH_4 concentration levels of 1000, 800, 600, 400, 200, 100, 50, and 0 ppbv. (b) Experimental data and fitting curve of CH_4 concentration versus max(2*f*). (c) Measured CH_4 concentration by passing pure N_2 into the MPGC for zero concentration. (d) Allan-Werle deviation plot as a function of averaging time, τ, based on the data shown in Fig. 6(c).

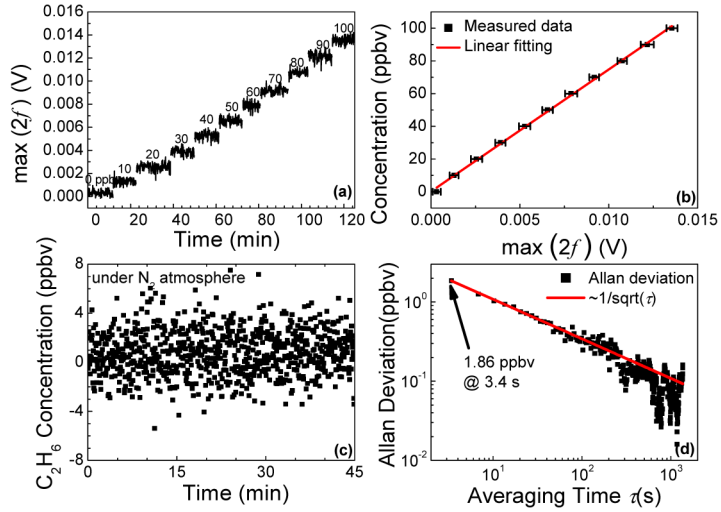

Fig. 7. (a) Measured 2*f* amplitude, max(2*f*), versus calibration time *t* for eleven C_2H_6 concentration levels of 0, 10, 20, 30, 40, 50, 60, 70, 80, 90, 100 ppbv. (b) Experimental data and fitting curve of C_2H_6 concentration versus max(2*f*). (c) Measured C_2H_6 concentration by passing pure N_2 into the MPGC for ~45 min. (d) Allan-Werle deviation plot as a function of averaging time, *τ*, based on the data shown in Fig. 7(c).

C_2H_6 sensor calibration was carried out by using diluted standard C_2H_6 sample with 11 different concentration levels of 0, 10, 20, 30, 40, 50, 60, 70, 80, 90 and 100 ppbv, as shown in Fig. 7(a). The measured amplitudes for each concentration was averaged and plotted as a

Optics EXPRESS

function of C_2H_6 concentration as shown in Fig. 7(b). The fitting curve indicates a good linear relationship (R-square value: 99.86%) between the 2*f* signal amplitude and C_2H_6 concentration, expressed as

$$C = 7762.23 \max_{C_2H_6}(2f) - 0.87, \text{ in ppbv} \quad (2)$$

Measurements of a C_2H_6 sample with 0 ppbv (pure N_2) over a period of ~45 min were performed. Figure 7(c) exhibits the measured concentration as a function of observation time *t*, and Fig. 7(d) shows the Allan-Werle deviation as a function of the averaging time τ. The Allan deviation is ~1.86 ppbv with a 3.4 s averaging time. With increasing averaging time, the Allan plot shows a continuous decrease, indicating that a white-noise dominated sensor was achieved for C_2H_6 detection.

4. Dual-gas sensing performance using a single CW ICL

The two absorption lines of CH_4 and C_2H_6 located at 2999.06 cm^{-1} and 2996.88 cm^{-1} were monitored for simultaneous concentration measurements of these two gases with a single ICL. The sensor system is the same as the one for single-gas detection as described in Section 3. For scanning the two lines, a special drive signal biased at ~2.0 V with a current range of 31–49 mA was applied to the ICL operating at 10 °C. This signal contained three parts. The first part and the third part were two ramp signals (amplitude: 200 mV, duration time: 5/3 s) superimposed by modulation signals (frequency: 5 kHz, amplitude: 0.024 V), which were used to scan the selected CH_4 line and the C_2H_6 line, respectively. The center part was an exponential signal used to connect the first part and the third part with a duration time of 2 s. Hence, the period of such a drive signal was ~4.3 s. The sampling rate and the integration time of the LabVIEW-based lock-in amplifier were the same as those used in single-gas detection. A pressure of 100 Torr inside the MPGC was selected for optimum sensor operation.

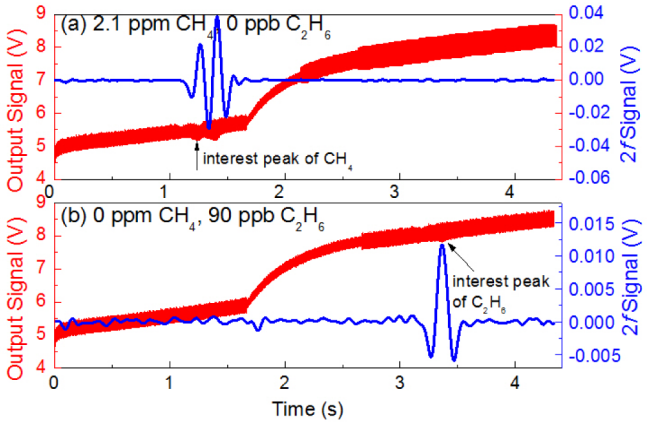

Fig. 8. Direct output signal from the MCT detector and demodulated 2*f* signal by the LabVIEW-based lock-in amplifier with a time constant of ~16 ms, (a) for a $CH_4/C_2H_6:N_2$ mixture with a CH_4 concentration of 2.1 ppmv and C_2H_6 concentration of 0 ppbv, and (b) for a prepared $CH_4/C_2H_6:N_2$ mixture with CH_4 concentration of 0 ppmv and C_2H_6 concentration of 90 ppbv.

The direct output signal from the detector and the demodulated 2*f* signal by the lock-in amplifier with a time constant of ~16 ms for the $CH_4/C_2H_6:N_2$ mixture with a CH_4 concentration of 2.1 ppmv and a C_2H_6 concentration of 0 ppbv are shown in Fig. 8(a). The two signals for the $CH_4/C_2H_6:N_2$ mixture with a CH_4 concentration of 0 ppmv and a C_2H_6 concentration of 90 ppbv are shown in Fig. 8(b). The two absorption peaks of CH_4 and C_2H_6 are included in both the absorption and the 2*f* signals with a single laser scan. The dual-gas

Optics EXPRESS

sensor was calibrated using the dilution of standard 2.1 ppmv CH_4 and 1.14 ppmv C_2H_6 concentrations. In the case of dual-gas detection, the linear relationships of the 2*f* signal amplitude as a function of the CH_4 and C_2H_6 concentrations are given Eq. (3) and Eq. (4), respectively

$$C_{CH_4} = 91.87 \max_{CH_4}(2f) - 0.0312, \text{ in ppmv} \quad (3)$$

$$C_{C_2H_6} = 8022.29 \max_{C_2H_6}(2f) - 2.8989, \text{ in ppbv} \quad (4)$$

The R-square values for the linear fitting in Eqs. (3) and (4) are 99.98% and 99.89%, respectively. There are some differences between the two relationship curves of Eq. (1) and Eq. (3) and also between the two curves of Eq. (2) and Eq. (4). This is because the long-term scan signal induced larger variations both in laser temperature and power compared with short-term scan for single-gas detection. Furthermore the baseline fitting algorithm was modified compared to the algorithm used in single-gas detection. These factors caused differences in the lock-in output between dual-gas and single-gas detection. In the following dual-gas detection, the calibration curves shown in Eqs. (3) and (4) were used in the sensor-performance evaluation of laboratory and outdoor CH_4/C_2H_6 measurements.

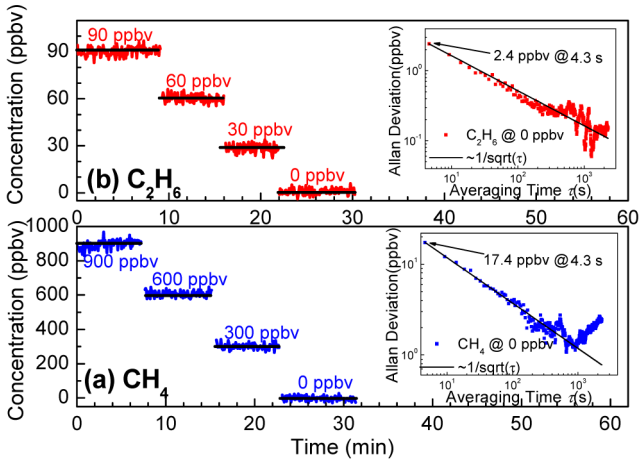

Fig. 9. Measurement results of concentration levels of (a) four CH4 samples (0, 300, 600, 900 ppbv) and (b) four C2H6 samples (0, 30, 60, 90 ppbv). The insets in Fig. 9(a) and 9(b) exhibit the Allan deviation plots obtained from long-term measurements on 0 ppmv CH4 and 0 ppbv C2H6 samples for ~40 min, respectively, using the calibrated dual-gas sensor system.

Both CH_4 and C_2H_6 detection performance were investigated using the calibrated dual-gas sensor. The concentration levels of four CH_4 samples (0, 300, 600, 900 ppbv) and four C_2H_6 samples (0, 30, 60, 90 ppbv) were measured using the sensor. The results are shown in Figs. 9(a) and 9(b). For an observation period of < 10 min, the dual-gas sensor was confirmed to have high accuracy with a small variation range of each measured concentration, i.e. ~ ± 30 ppbv for CH_4, ~ ± 5 ppbv for C_2H_6. Long-term measurements for 0 ppmv CH_4 and 0 ppbv C_2H_6 were conducted for ~40 min. The Allan deviations were obtained and shown as insets of Figs. 9(a) and 9(b), respectively. The Allan deviations for the two gases were 17.4 ppbv for CH_4 and 2.4 ppbv for C_2H_6 for an averaging time of 4.3 s. These two values are slightly larger than those obtained from the single-gas detection, i.e. 11.2 ppbv @ 3.4 s for CH_4 (Fig. 6) and 1.86 ppbv @ 3.4 s for C_2H_6 (Fig. 7) for a 45-minute observation time period. Furthermore, the Allan deviation for dual-gas detection starts to increase after an integration time of > 100 s, which indicates the appearance of a system drift. This seems to indicate that the dual-gas

Optics EXPRESS

sensor shows a small decrease in stability in CH_4 and C_2H_6 detection compared to a single-gas sensor system.

The detection characteristic of the dual-gas sensor was further assessed using three generated C_2H_6 samples (90, 50 and 0 ppbv) using an Environics gas dilution system (Environics, Series 4040) and the standard 2.1 ppmv CH_4 sample. Two valves were used to switch between the two gas streams into the MPGC (Fig. 10(c)). Three exchanges were made between the two gas streams as shown in Fig. 10(a). A detailed illustration of the measurement results during the 2nd gas stream exchange is shown in Fig. 10(b). A response time of < 40 s was required to complete the exchange for a gas flow of about 45 ml/min. These results demonstrate the normal operation of the dual-gas sensor for monitoring both CH_4 and C_2H_6 simultaneously.

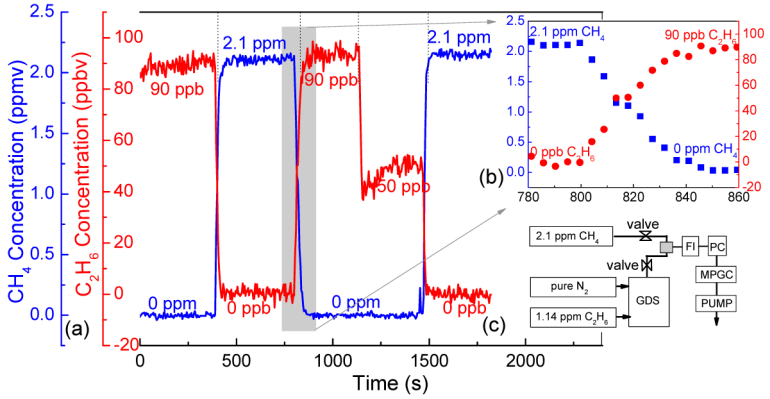

Fig. 10. (a) CH_4/C_2H_6:N_2 concentration measurements using the dual-gas sensor system described in Section 2 and 4. (b) Detailed illustration of the measured concentration during the 2nd exchange between CH_4 and C_2H_6 streams. (c) Schematic diagram of a CH_4/C_2H_6 mixing setup based on the C_2H_6 samples by the gas dilution system (GDS) and a standard 2.1 ppmv CH_4 sample. FI: flow indicator; PC: pressure controller; MPGC: multipass gas cell.

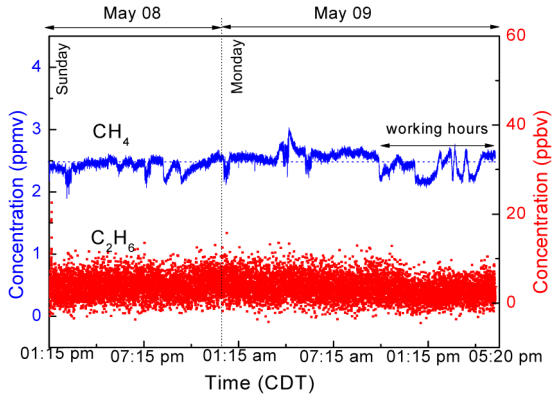

Fig. 11. Simultaneously measured concentrations of CH_4 and C_2H_6 in ambient air during ~28 hours period on May 8-9, 2016 inside the Laser Science Laboratory (located in Space Science Technology building, Rice University).

5. Atmospheric CH_4/C_2H_6 detection

5.1 Indoor measurements

The sensor system was evaluated for the simultaneous measurements of C_2H_6 and CH_4 concentrations in a laboratory environment (in the Rice Laser Science Laboratory, SST 104). Measured concentrations of C_2H_6 and CH_4 from 13:15 CDT, May 08, 2016 to 17:20 CDT,

Optics EXPRESS

May 09, 2016) are displayed in Fig. 11. It is observed that the concentration of C_2H_6 was relatively constant during this period of time, with an average of ~3.4 ± 2.5 ppbv (1σ). The average CH_4 concentration level was ~2.48 ± 0.14 ppmv (1σ). These variations in the CH_4 concentration level were obvious during the working hours on Monday (May 09, 2016). The CH_4 concentration exhibited relatively minor variation during the period of monitoring (relative standard deviation ~5.5%), with slight increase during the early morning hours followed by decreasing concentrations during the day, as observed by previous studies [21].

5.2. Outdoor measurements

The sensor system was also evaluated for simultaneous detection of atmospheric CH_4 and C_2H_6 on the Rice University campus. For outdoor measurements, the dual trace gas sensor system was mounted on a cart and power was supplied by a battery (Power-Sonic, model PG-12V150-FR) connected to an AC inverter (Wagan Tech, model 9622). The photograph, shown in Fig. 12(a), of the sensor system was taken when it was placed outside the Laser Science Laboratory (SST 104) to monitor variations of atmospheric CH_4 and C_2H_6 concentrations. For continuous day and night monitoring, the cart was placed inside the laboratory and the outside air was pumped into the gas cell using a long sampling line. The measured concentrations are plotted in Fig. 12(b). The experiment was conducted from 16:13 CDT on May 6, 2016 to 10:55 CDT on May 8, 2016 (~67 hours sampling). Fluctuations in concentration levels were observed during atmospheric monitoring of CH_4 and C_2H_6. The C_2H_6 concentration ranged between 0 and 44 ppbv, with an average value of 6.4 ± 5.5 ppbv. The CH_4 concentration varied from 2.1 to 4.4 ppmv, with an average value of 2.6 ± 0.4 ppmv. CH_4 concentrations were above 4 ppmv during the early morning hours and then dropped gradually to its typical urban background level of ~2.1–2.4 ppmv. The detected CH_4 concentration levels exhibited the typical hourly profile expected for this gas species which is related with boundary layer dynamics and the extent of mixing in the atmosphere [1]. C_2H_6 concentrations peaked during early morning hours resembling diurnal trends observed for CH_4 during the sampling period. Furthermore, point emission sources of CH_4 and C_2H_6 in the Greater Houston area might be responsible for minor concentration peaks observed during the period of monitoring.

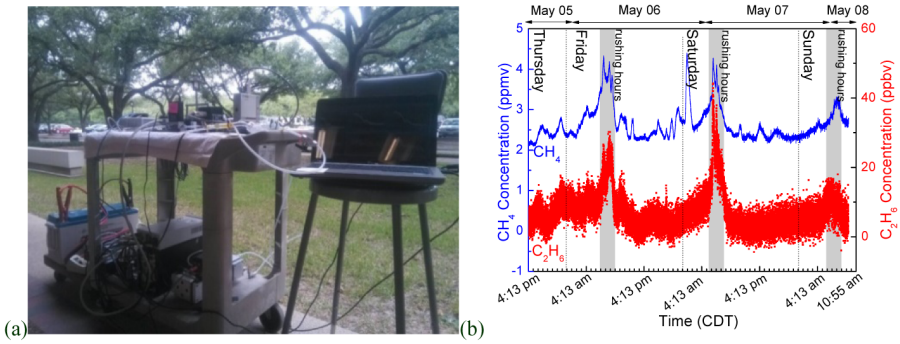

Fig. 12. (a) Single CW ICL based dual-gas CH_4/C_2H_6 sensor system installed on a laboratory cart. (b) Measurement results of simultaneous CH_4 and C_2H_6 monitoring in the atmosphere for ~67 hours time duration on the Rice University campus.

6. Conclusions

A sensitive and selective sensor system based on a single CW DFB ICL was demonstrated for simultaneous detection of CH_4 and C_2H_6. The sensor system was based on TDLAS and 2*f*-WMS detection methods. An ICL with a wavelength of ~3.337 μm was employed to target the two absorption lines of both CH_4 and C_2H_6 within a narrow spectral range of ~3 cm^{-1}. A compact MPGC with an effective optical path length of 54.6 m was used to enhance the gas

Optics EXPRESS

absorption. The sensor system was first evaluated for individual CH_4 and C_2H_6 detection, with the ICL wavelength tuned to each gas absorption line center. An Allan deviation analysis yielded detection sensitivities of 11.2 ppbv for CH_4 and 1.86 ppbv for C_2H_6 for an integration time of 3.4 s. Subsequently, the sensor system was evaluated for simultaneous CH_4 and C_2H_6 detection using the same ICL. The detection sensitivities increased slightly to 17.4 ppbv for CH_4 and 2.4 ppbv for C_2H_6 for an averaging time of 4.3 s due to the increased drift in both laser temperature and power caused by the longer scanning time periods. Measurement results for both indoor and outdoor atmospheric concentration changes of these two gases were also reported. The demonstrated dual-gas sensor architecture shows the merits of simultaneous CH_4 and C_2H_6 detection with a single sensor of significantly reduced size and cost without influencing the mid-infrared sensor detection sensitivity, selectivity and reliability.

Funding

National Science Foundation (NSF) (ERC MIRTHE award); USA Robert Welch Foundation (C-0586); NSF Phase II SBIR (IIP-1230427DE DE); DOE ARPA-E awards (DE-0000545, DE-0000547); National Natural Science Foundation of China (NSFC) (61307124, 61575113, 61275213); Changchun Municipal Science and Technology Bureau (14KG022); High School Outstanding Young Teacher Training Program of Guangdong Province (YQ2015071); China Scholarship Council (201506175025, 201508440112).